Determination of the statistical distribution of electromagnetic-field amplitudes in complex cavities

R. H. Price, H. T. Davis, and E. P. Wenaas
JAYCOR, 700 Comanche Road, N.E., Albuquerque, New Mexico 87107
(Received 12 March 1993)

We describe an analytic technique to predict the statistical distribution of field amplitudes in complex cavities, which result from the simultaneous excitation of hundreds of modes. We have been able to determine that the electromagnetic-field amplitudes in a complex cavity are statistically distributed according to a Γ distribution. The shape of the distribution depends on a dimensionless parameter, the specific mode density, which is a measure of the number of modes excited simultaneously in the cavity. In the limit of large cavity volume, measured in cubic wavelengths, and of moderate to low Q, the distribution becomes a χ^2 distribution with a uniform shape, independent of cavity parameters. Comparison with experimental data is included for four real systems widely varying in size, shape, and Q, and with a laboratory experiment which varied the cavity Q in a controlled manner over two orders of magnitude. In all these cases the data fell within the 90% confidence bounds of the theory. The theory further provides a quantitative measure capable of distinguishing to what extent experimental data have been distorted by the finite dynamic range of the measurement instrumentation, and of restoring the correct statistics in spite of large distortions in the data. This measure does not depend on knowledge of the instrumentation system. Errors less than several decibels appear detectable.

PACS number(s): 03.50.De, 05.20.Gg, 41.20.Jb, 84.90.+a

INTRODUCTION

For many years microwave transfer functions and coupling cross sections have been measured for military assets, such as trucks, tanks, airplanes, etc. The measured functions are extremely complex and appear exquisitely sensitive to variations in angle of incidence, frequency, mechanical configuration, and other parameters. More recently it was recognized empirically that the cumulative distribution function of measured fields or coupling cross sections was much less sensitive to experimental parameters (Ref. [1]), and in fact was recognized by some (Ref. [2]) as a "universal" curve. However, to date no theoretical basis or justification has been available to support this observation. It is now possible to provide the required theoretical justification.

The complex nature of the measured transfer functions and coupling cross section has been attributed to a variety of phenomena, including variations in resonance amplitude, coupling to the cavity, cavity Q, and others. Each of these undoubtedly contains an element of truth, but cannot itself account for the observed behavior. In many of the real, nonideal, cavities measured in experiments, the Q is determined mainly by wall losses and aperture losses. In nonpathological cases these losses should vary by only a factor of a few between modes, and thus are unable to account for the many-order-of-magnitude variation observed. Similarly, aperture resonances are typically low Q, less than about 30, and thus do not vary rapidly enough in frequency or greatly enough in amplitude to account for the observed data by themselves. Some other phenomena must be responsible for the greater portion of the observed behavior. We present evidence to the effect that the principal phenomenon responsible for the observed characteristics of transfer functions and coupling cross sections is the statistical nature of a measurement made at a single spatial location in a complex, irregular cavity, containing many modes simultaneously excited.

As in many problems in physics the solution hinges on a clear definition of what is being measured and how the measurement is made. One can imagine a cavity in which a single mode is excited and a sensor is located at a fixed but arbitrary location. For concreteness we deal with a B-dot-sensor measurement, but the sensor could be an electric dipole or any other field sensor. Since the B-dot-sensor is at an arbitrary location relative to the peaks and nodes of the mode, it may measure a field strength with any value between the true mode amplitude and zero. If one changes the frequency slightly and excites a different mode, the spatial pattern will jump to a new configuration, and the sensor will be at a different position relative to the peaks and nodes. The sensor will again measure a field strength greater than zero and less than or equal to the true mode amplitude, and unrelated to that of the previous mode. Thus, far from measuring the mode amplitude, in any few measurements the sensor only measures samples greater than zero and less than the true mode amplitude by some unknown amount. The true mode amplitude remains undetermined, as does the energy density in the cavity and the maximum field that a sensor or component might experience at some other location in the cavity. The other location might coincide with the peak of a mode, yielding a much higher field strength.

In reality this picture is further complicated by the fact that in most real cavities many modes are excited simultaneously. The field at a particular location may be the sum of contributions of hundreds of modes. Furthermore, coupling to the sensor is polarization dependent

and the polarizations of the many modes are undetermined. In irregular cavities with nonorthogonal walls the field polarization for a given mode can vary with spatial location. All this leads to the recognition that an exact treatment of the problem to calculate the fields in a cavity of a particular shape, at a particular location, and with the many other required parameters specified, is both hopelessly complex and equally useless. Any change in any of the parameters requires a new complex solution and leaves no general understanding of the behavior of the system. A useful solution to this problem must be statistical in nature and depend only on general properties of the system. This is an intuitively satisfying conclusion. The solution cannot depend in detail on such things as whether a small metallic can has been set down somewhere inside the test article, or the position of the pilot's arms, or whether some mechanical widget has moved from position A to position B, changing the mode structure. If the answer did depend on those things, all of the measurements would be useless, defeated by the minutiae present in all systems.

SPECIFIC MODE DENSITY

Intuitively one would expect the statistical behavior of the cavity fields to depend on the number of modes excited simultaneously. This appears to be the case. The number of excited modes can be easily estimated. The mode density for a cavity is

$$\frac{dN}{d\nu}d\nu=\frac{8\pi V}{c^3}\nu^2 d\nu \ , \tag{1}$$

where V is the cavity volume, c is the speed of light, ν is the frequency, and dN is the number of modes in the band $d\nu$ at frequency ν. The derivation of the mode density is exactly analogous to the derivation of the mode density used in blackbody radiation calculations and many other quantum problems, and can be found in detail in any textbook (Ref. [3]) covering blackbody radiation. In connection with blackbody radiation it has been shown that the mode density does not depend on the shape of the cavity, only on its volume. (Certain nonsimply connected, pathological shapes must be excluded from consideration.) If the cavity is excited by a relatively monochromatic source the bandwidth in which the modes will be excited is set by the average cavity Q:

$$\Delta\nu=\frac{\nu}{Q} \ . \tag{2}$$

Combining Eqs. (1) and (2) gives the characteristic number of modes simultaneously excited in the cavity:

$$N_s=\frac{8\pi V}{\lambda^3 Q} \ . \tag{3}$$

We call this quantity the specific mode density. It is a dimensionless quantity characteristic of a particular cavity excited at a given frequency. In reality, numerous modes in a cavity are excited to a greater or lesser degree, but the specific mode density is a measure of the number of modes which contain the majority of the energy in the cavity.

MEASURED POWER IN AN OVERMODED CAVITY

The electric and magnetic fields in a cavity can be decomposed into contributions from each of the cavity's eigenmodes so that the cavities internal fields can be written as

$$\begin{aligned}\mathbf{B}(\mathbf{r},t)&=\sum_i \mathbf{B}_i(\mathbf{r},t) \ ,\\ \mathbf{E}(\mathbf{r},t)&=\sum_i \mathbf{E}_i(\mathbf{r},t) \ .\end{aligned} \tag{4}$$

Each of the eigenmodes satisfies Maxwell's equations for the cavity and its boundary conditions. The explicit coordinate system chosen is not important since only the general properties of the eigenmodes are important for this problem. The system is assumed to be in steady state or slowly varying, and all transient modes have died out. These assumptions may not be rigorously required, but are made to simplify the derivation. We separate each eigenmode into the product of five functions, each of which has different properties. These functions are not separated by coordinates and do not require a separable coordinate system. The magnetic and electric fields for the ith eigenmode can be written as

$$\begin{aligned}\mathbf{B}_i(\mathbf{r},t)&=B_{0i}(\omega)\hat{\mathbf{b}}_i(\mathbf{r})g_i(\mathbf{r})f_i(\mathbf{r})\sin(\omega t+\phi_i) \ ,\\ \mathbf{E}_i(\mathbf{r},t)&=E_{0i}(\omega)\hat{\mathbf{e}}_i(\mathbf{r})g_i(\mathbf{r})h_i(\mathbf{r})\cos(\omega t+\phi_i) \ .\end{aligned} \tag{5}$$

The first function, $B_{0i}(\omega)$, is the scalar amplitude of the magnetic field of the ith eigenmode averaged over the cavity volume, such that

$$U_i=\frac{B_{0i}^2}{8\pi}V \ , \tag{6}$$

where U_i is the total energy in the cavity in the ith eigenmode. The second function, $\hat{\mathbf{b}}_i$, is a unit vector which points along the magnetic field of the ith mode at each point in the cavity. The third function, g_i, is the slowly varying part of the spatial distribution. It can be obtained by taking the square of the spatially dependent magnitude of the original ith eigenmode and averaging it over a half-wavelength-radius volume at each point in the cavity, as follows:

$$g_i(\mathbf{r}')=\left[\frac{2}{B_{0i}^2}\int_{V_{\rm ph}(\mathbf{r}')}\mathbf{B}_i^2(\mathbf{r},t)d\mathbf{r}\,dt\right]^{1/2} \ , \tag{7}$$

where $V_{\rm ph}$ is the phase volume, a sphere one half wavelength in radius centered at $\mathbf{r}'$. The new function, g_i, is smoothly varying, without rapid oscillations everywhere in the volume. Further, it is normalized so the average throughout the volume is unity. The fourth function, f_i, is the rapidly varying part of the original ith eigenfunction. It is obtained by taking the spatially dependent magnitude of the ith eigenfunction and dividing it by $B_{0i}(\omega)$ and $g_i(\mathbf{r})$, as follows:

$$f_i(\mathbf{r})=\frac{2\hat{\mathbf{b}}_i(\mathbf{r})\cdot\overline{\mathbf{B}_i(\mathbf{r},t)\sin(\omega t)}}{B_{0i}g_i(\mathbf{r})} \ , \tag{8}$$

where the overbar indicates a time average. The fifth

function is just the time dependence of the ith eigenmode including its phase, ϕ_i. The frequency is determined by the external exciting field and is the same for all excited modes. The functions describing the electric field have analogous definitions. The electric-field magnitude, $E_{0i}(\omega)$, is identically equal to $B_{0i}(\omega)$. This means that the electric and magnetic energy in the cavity are equal, and each is one half of the total energy stored in the cavity. We explicitly assume, for simplicity, that there is no static electric field. Beyond this point the electric field is ignored as we are considering a B-dot sensor. The treatment of an electric-field sensor is exactly analogous, and the results for one apply to the other by simply substituting the appropriate effective area (antenna cross section) for the sensor.

GENERAL PROPERTIES OF THE EIGENFUNCTION COMPONENTS

While many relationships between the various defined functions can be derived from Maxwell's equations we present only those relevant to this problem. First the integral of g_i^2 over the cavity volume is equal to the volume, which results in

$$\frac{1}{V}\int_V g_i^2(\mathbf{r})d\mathbf{r}=1 \ . \tag{9}$$

This is required by the earlier definition for $B_{0i}(\omega)$, which stated that it was the volume average magnetic field. Next, the integral of $f_i(r)$ squared, over the phase volume, is unity:

$$\int_{V_{\rm ph}(\mathbf{r}')} f_i^2(\mathbf{r})d\mathbf{r}=1 \ . \tag{10}$$

Finally, the eigenfunctions form an orthogonal basis set:

$$\int_V \hat{\mathbf{b}}_i g_i f_i \cdot \hat{\mathbf{b}}_k g_k f_k d\mathbf{r}=V\delta_{ik} \ , \tag{11}$$

where δ_{ik} is a Kronecker δ function. We assume that the energy density of the field is measured at a particular location $\mathbf{r}'$, by a B-dot sensor with physical area a. Its area vector is written as

$$\mathbf{a}=\hat{\mathbf{a}}a\,\delta(\mathbf{r}-\mathbf{r}') \ , \tag{12}$$

where $\hat{\mathbf{a}}$ is a unit vector pointing along the axis of greatest sensitivity of the B-dot sensor, and $\delta(\mathbf{r}-\mathbf{r}')$ is a Dirac δ function. The power measured by a square-law detector is

$$P_s=10^{-9}\frac{\omega^2}{R}\overline{[\mathbf{a}\cdot\mathbf{B}(\mathbf{r},t)]^2} \ , \tag{13}$$

where R is the sensor load impedance in ohms. This can easily be related to the sensor's free field cross section, which is

$$\sigma_s=\frac{P_s}{S}=4\pi\times 10^{-9}\frac{a^2\omega^2}{Rc} \ , \tag{14}$$

where P_s is the power measured by the sensor in ergs/sec, and S is the incident power density in ergs/sec cm^2. It has been assumed that the sensor axis has been aligned to the magnetic field for maximum coupling. Equation (13) can be rewritten in terms of the sensor maximum free field cross section.

$$P_s=\frac{\sigma_s c}{4\pi}\overline{[\hat{\mathbf{a}}_j\cdot\mathbf{B}(\mathbf{r}_s,t)]^2} \ . \tag{15}$$

The power measured can now be expanded in terms of the functions defined above, as follows:

$$\begin{aligned}P_s&=\frac{\sigma_s c}{4\pi}\left[\sum_i B_{0i}(\hat{\mathbf{a}}\cdot\hat{\mathbf{b}}_i)g_i f_i\sin(\omega t+\phi_i)\right]^2\\&=\frac{\sigma_s c}{8\pi}\left[\sum_i B_{0i}^2(\hat{\mathbf{a}}\cdot\hat{\mathbf{b}}_i)^2 g_i^2 f_i^2+\sum_{\substack{i,k\\ i\neq k}} B_{0i}B_{0k}(\hat{\mathbf{a}}\cdot\hat{\mathbf{b}}_i)(\hat{\mathbf{a}}\cdot\hat{\mathbf{b}}_k)g_i g_k f_i f_k\cos(\phi_i-\phi_k)\right] .\end{aligned} \tag{16}$$

It is important to note at this point that when the volume integral of the field is taken over the cavity volume, the cross terms of the eigenmodes integrate to zero from the orthogonality condition Eq. (11). When the field is measured at a local point the cross terms are not equal to zero. It is the cross terms which produce the complex spiky nature of the transfer functions and circuit cross sections.

CAVITY RATE EQUATION AND RESONANCE FUNCTION

The rate equation for the total energy in the cavity in the ith mode is

$$\frac{dU_i}{dt}+\frac{\omega_i}{Q_i}U_i=\frac{\left[\frac{\omega_i}{2Q_i}\right]^2\epsilon_i P_c}{(\omega-\omega_i)^2+\left[\frac{\omega_i}{2Q_i}\right]^2} \ ; \tag{17}$$

in steady state we have

$$\begin{aligned}U_i&=\frac{\frac{\omega_i}{4Q_i}\epsilon_i P_c}{(\omega-\omega_i)^2+\left[\frac{\omega_i}{2Q_i}\right]^2}\\&=\frac{V}{8\pi}B_{0i}^2(\omega) \ ,\end{aligned} \tag{18}$$

where ϵ_i is the random coupling coefficient for the ith mode to the cavity, given by $\epsilon_i = P_i / P_c$. The P_i is the power that is coupled into the ith mode, and the P_c is the total power coupled into the cavity. The random variable ϵ_i is the random part of B_{0i}, and the ensemble satisfies

$$\sum_i \epsilon_i = 1 \ . \tag{19}$$

That is, the energy coupled into the cavity is fixed, and the independent and identically distributed ϵ_i are "gap" statistics (Ref. [4]).

The resonance function on the right-hand sides of Eqs. (17) and (18) is only an approximation which is valid near resonance (Ref. [5]). The actual resonance function is truncated a finite distance in frequency above and below resonance. It does not extend to plus and minus infinity. This fact is important to the convergence of certain sums and integrals which occur later in this paper.

STATISTICAL PROPERTIES OF THE MEASURED POWER AND ITS COMPONENT FUNCTIONS

We wish to determine the statistical properties of P_s, which includes the form of the distribution, and the parameters which determine its shape. From Eqs. (13), (15), and (16) it is clear that P_s is positive definite and of quadratic form. The random vector f_i is shown in Eq. (8) to be a time average of a stationary process. The central limit theorem assures that the vector has an asymptotic Gaussian distribution. The asymptotic distribution of the quadratic form can then be approximated by a Γ distribution (Refs. [6,7]) with probability density:

$$f(x) = \frac{x^{\alpha-1} e^{-x/\beta}}{\Gamma[\alpha]\beta^{\alpha}}, \quad 0 \le x < \infty \ . \tag{20}$$

The mean of the distribution is

$$\mu = \alpha\beta = E(P_s) \tag{21}$$

and the variance is

$$\sigma^2 = \alpha\beta^2 = \mu\beta = E(P_s^2) - [E(P_s)]^2 \ , \tag{22}$$

where $E(\ )$ indicates the expectation value, and σ, the standard deviation, is to be distinguished from σ_s, the B-dot cross section.

The mean and variance of the measured power can be determined in terms of the mean and variance of the functions which are components of Eq. (16). For functions which are independent, the mean of the function is just the product of the means of its component functions. The variances are treated similarly. One must use care to determine that the functions are in fact independent. In Eq. (16) the amplitude and the phase are not independent. The expectation value of the measured power $E(P_s)$ can be expanded as

$$E(P_s) = \frac{\sigma_s c}{8\pi} \left[\sum_i E(B_{0i}^2) E((\hat{\mathbf{a}}\cdot\hat{\mathbf{b}}_i)^2) E(g_i^2) E(f_i^2) + \sum_{\substack{i,k \\ i\neq k}} E(B_{0i}B_{0k}\cos(\phi_i - \phi_k)) E(\hat{\mathbf{a}}\cdot\hat{\mathbf{b}}_i) E(\hat{\mathbf{a}}\cdot\hat{\mathbf{b}}_k) E(g_i) E(g_k) E(f_i) E(f_k) \right] . \tag{23}$$

The expectation value of the square of P_s can be expanded as follows:

$$E(P_s^2) = \left[\frac{\sigma_s c}{8\pi} \right]^2 [E(T_1) + E(T_2) + E(T_3)] \ , \tag{24}$$

where

$$E(T_1) = E\left[\left[\sum_i B_{0i}^2 (\hat{\mathbf{a}}\cdot\hat{\mathbf{b}}_i)^2 g_i^2 f_i^2 \right]^2 \right] = \sum_k E(B_{0k}^4) E((\hat{\mathbf{a}}\cdot\hat{\mathbf{b}}_k)^4) E(g_k^4) E(f_k^4) + \sum_{\substack{k,l \\ k\neq l}} E(B_{0k}^2 B_{0l}^2) E((\hat{\mathbf{a}}\cdot\hat{\mathbf{b}}_k)^2) E((\hat{\mathbf{a}}\cdot\hat{\mathbf{b}}_l)^2) E(g_k^2 g_l^2) E(f_k^2) E(f_l^2) \ , \tag{25}$$

$$E(T_2) = 2 \sum_{\substack{k,l \\ k\neq l}} \sum_i E(B_{0i}^2 B_{0k} B_{0l} \cos(\phi_l - \phi_k)) E((\hat{\mathbf{a}}\cdot\hat{\mathbf{b}}_i)^2) E(\hat{\mathbf{a}}\cdot\hat{\mathbf{b}}_k) E(\hat{\mathbf{a}}\cdot\hat{\mathbf{b}}_1) E(g_i^2 g_k g_l) E(f_i^2) E(f_k) E(f_l) \ , \tag{26}$$

$$E(T_3) = \sum_{\substack{k,l \\ k\neq n}} \sum_{\substack{m,n \\ m\neq n}} E(B_{0k} B_{0l} B_{0m} B_{0n} \cos(\phi_k - \phi_l) \cos(\phi_m - \phi_n)) E((\hat{\mathbf{a}}\cdot\hat{\mathbf{b}}_k)(\hat{\mathbf{a}}\cdot\hat{\mathbf{b}}_l)(\hat{\mathbf{a}}\cdot\hat{\mathbf{b}}_m)(\hat{\mathbf{a}}\cdot\hat{\mathbf{b}}_n)) E(g_k g_l g_m g_n) E(f_k f_l f_m f_n) \ . \tag{27}$$

The expectation values of many of the component functions can be easily determined. First the polarization vectors in a complex, nonorthogonal cavity are assumed to be randomly oriented. To find the expectation values of the polarization-dependent functions we establish a spherical coordinate system with the z axis along $\hat{\mathbf{a}}_j$. θ is the angle between the polarization vector and the z axis. The probability density for finding a particular value of θ is

$$P(\theta)d\theta=\tfrac{1}{2}\sin(\theta)d\theta, \quad 0\le\theta\le\pi \ . \tag{28}$$

The polarization functions can then be written in terms of

$$\hat{\mathbf{a}}\cdot\hat{\mathbf{b}}_i=\cos(\theta) \ . \tag{29}$$

Each of three required polarization expectation values can be determined as follows:

$$E(\hat{\mathbf{a}}\cdot\hat{\mathbf{b}}_i)=\tfrac{1}{2}\int_0^{\pi}\cos(\theta)\sin(\theta)d\theta=0 \ , \tag{30}$$

$$E((\hat{\mathbf{a}}\cdot\hat{\mathbf{b}}_i)^2)=\tfrac{1}{2}\int_0^{\pi}[\cos(\theta)]^2\sin(\theta)d\theta=\tfrac{1}{3} \ , \tag{31}$$

$$E((\hat{\mathbf{a}}\cdot\hat{\mathbf{b}}_i)^4)=\tfrac{1}{2}\int_0^{\pi}[\cos(\theta)]^4\sin(\theta)d\theta=\tfrac{1}{5} \ . \tag{32}$$

The f_i functions are rapidly oscillating and constrained by the normalization condition in Eq. (10). The expectation values for f_i and its square follow directly:

$$E(f_i)=\frac{\int_V f_i d\mathbf{r}}{\int_V d\mathbf{r}}=0 \ , \tag{33}$$

$$E(f_i^2)=\frac{\int_V f_i^2 d\mathbf{r}}{\int_V d\mathbf{r}}=1 \ . \tag{34}$$

The expectation value for the fourth power of f_i cannot be found exactly for a general eigenfunction, however, it can be approximated by the range of values it takes on in a rectangular box. This calculation is given in the Appendix. This can be thought of as a local approximation in the region of the measurement point. The required approximation for the expectation value is

$$E(f_i^4)=\frac{\int_V f_i^4 d\mathbf{r}}{\int_V d\mathbf{r}}\approx\tfrac{5}{2} \tag{35}$$

and it can be further shown that the expectation can be bounded by $\frac{11}{8}\le E(f_i^4)\le\frac{27}{8}$. The approximation for the expectation value depends on neither the dimensions of the volume nor the integer values selecting the specific mode, as one would anticipate. It can be seen at this point that the second term in Eq. (23) is zero from Eqs. (30) and (33). Two expectation values in Eq. (23) remain to be determined. The first is

$$\sum_i E(B_{0i}^2)=E\left[\sum_i B_{0i}^2\right]=\sum_i \frac{\frac{\omega_i}{4Q}P_c\bar{\epsilon}}{(\omega-\omega_i)^2+\left[\frac{\omega_i}{2Q}\right]^2}$$

$$=\frac{8\pi}{V}U \ , \tag{36}$$

where we have used Eq. (6), U is the total energy in all modes in the cavity, and $\bar{\epsilon}$ is the mean value of the ϵ_i. The sum in Eq. (36) can be approximated by a Rieman integral, using the density of modes in Eq. (3):

$$E\left[\sum_i B_{0i}^2\right]\approx\int\frac{2\pi\bar{\epsilon}P_c\frac{\omega_k}{VQ}}{(\omega-\omega_i)^2+(\omega/2Q)^2}\frac{8\pi V}{(2\pi c)^3}\omega_i^2 d\omega_i$$

$$\approx\frac{4\bar{\epsilon}P_c\omega^2}{c^3} \ . \tag{37}$$

Details of the integration are carried out in the Appendix.

The second expectation to be evaluated is

$$E(g_i^2)=[g(\mathbf{r})]^2 \ . \tag{38}$$

Since g_i is a smooth, slowly varying function of position in the cavity, its expectation value, $g(\mathbf{r})$, is just a geometrical factor which represents the ratio of the local energy density to the average energy density. It is a slowly varying function of both location and frequency. By ergodicity and Eq. (9), if $g^2(\mathbf{r})$ is averaged over many spatial locations its average is unity. Also, since the variance of a slowly varying function is small, it also follows that $E[g]\approx E[g^2]$, hence

$$\begin{aligned} &E(g(\mathbf{r}))\approx 1 \ , \\ &E(g^2(\mathbf{r}))=1 \ . \end{aligned} \tag{39}$$

Equation (23) now becomes

$$E(P_s)=\sigma_s\frac{Uc}{3V} \tag{40}$$

and Eq. (21) becomes

$$\mu=\alpha\beta=\sigma_s\frac{Uc}{3V} \ . \tag{41}$$

Equations (40) and (41) relate the mean value of a transfer function to the total energy in the cavity and to the parameters for the probability density function in Eq. (20).

We now turn to evaluate Eqs. (24)–(27). From Eqs. (30) and (33) it immediately follows that Eq. (26) is zero:

$$E(T_2)=0 \ . \tag{42}$$

It is also obvious from Eqs. (30)–(35) that only terms with even powers of the polarization or f_i functions are nonzero. This fact can be used to reduce Eq. (27), since the only terms where $k=m$ and $l=n$ or $k=n$ and $l=m$ are nonzero: Eq. (27) becomes

$$E(T_3)=2E\left[\sum_{\substack{k,l\\k\neq l}} B_{0k}^2 B_{0l}^2\cos^2(\phi_k-\phi_l)\right]E((\hat{\mathbf{a}}\cdot\hat{\mathbf{b}}_k)^2)E((\hat{\mathbf{a}}\cdot\hat{\mathbf{b}}_l)^2)E(g_k^2)E(g_l^2)E(f_k^2)E(f_l^2)$$
$$=\tfrac{2}{9}g^4E\left[\sum_{\substack{k,l\\k\neq l}} B_{0k}^2 B_{0l}^2\cos^2(\phi_k-\phi_l)\right]. \tag{43}$$

Equation (25) can also be reduced at this point:

$$E(T_1)=E\left[\left[\sum_i B_{0i}^2(\hat{\mathbf{a}}\cdot\hat{\mathbf{b}}_i)^2 g_i^2 f_i^2\right]^2\right]$$
$$=E\left[\sum_k B_{0k}^4 E((\hat{\mathbf{a}}\cdot\hat{\mathbf{b}}_k)^4)E(g_k^4)E(f_k^4)\right]+E\left[\sum_{\substack{k,l\\k\neq l}} B_{0k}^2 B_{0l}^2 E((\hat{\mathbf{a}}\cdot\hat{\mathbf{b}}_k)^2)E((\hat{\mathbf{a}}\cdot\hat{\mathbf{b}}_l)^2)E(g_k^2)E(g_l^2)E(f_k^2)E(f_l^2)\right]$$
$$=\tfrac{1}{2}g^4E\left[\sum_k B_{0k}^4\right]+\tfrac{1}{9}g^4E\left[\sum_{\substack{k,l\\k\neq l}} B_{0k}^2 B_{0l}^2\right]. \tag{44}$$

Combining Eqs. (24), (42), (43), and (44) we obtain

$$E(P_s^2)=\left[\frac{c\sigma_s g^2}{8\pi}\right]^2\left[\frac{1}{2}E\left[\sum_k B_{0k}^4\right]+\frac{1}{9}E\left[\sum_{\substack{k,l\\k\neq l}} B_{0k}^2 B_{0l}^2\right]+\frac{2}{9}E\left[\sum_{\substack{k,l\\k\neq l}} B_{0k}^2 B_{0l}^2\cos^2(\phi_k-\phi_l)\right]\right]. \tag{45}$$

Using Eqs. (36) and (40) we obtain

$$[E(P_s)]^2=\left[\frac{c\sigma_s g^2}{8\pi}\right]^2\left[\frac{1}{9}\sum_k[E(B_{0k}^2)]^2+\frac{1}{9}E\left[\sum_{\substack{k,l\\k\neq l}} B_{0l}^2 B_{0k}^2\right]\right]. \tag{46}$$

Equation (22) for the variance can be rewritten using Eqs. (45) and (46):

$$\sigma^2=E(P_s^2)-[E(P_s)]^2$$
$$=\left[\frac{c\sigma_s g^2}{8\pi}\right]^2\left[\frac{1}{2}E\left[\sum_k B_{0k}^4\right]+\frac{2}{9}E\left[\sum_k\sum_l B_{0k}^2 B_{0l}^2\cos^2(\phi_k-\phi_l)\right]-\frac{1}{3}\sum_k[E(B_{0k}^2)]^2\right], \tag{47}$$

where it is important to note that in the second term the summation has changed from k not equal to l to the sum over all k and l.

The remaining expectation values in Eq. (47) are more difficult, but may be evaluated using the Riemann approximation converting the sum to an integral. Using Eqs. (1), (6), and (18) we can convert the first expectation value as follows:

$$E\left[\sum_k B_{0k}^4\right]=\sum_k\left[\frac{\frac{2\pi\omega_k}{VQ_k}P_c}{(\omega-\omega_k)^2+(\omega_k/2Q_k)^2}\right]^2 E[\epsilon_k^2]$$
$$\approx\mu_2\int_{\omega-\Omega}^{\omega+\Omega}\frac{\left[2\pi P_c\frac{\omega_k}{Q_k V}\right]^2}{[(\omega-\omega_k)^2+(\omega_k/2Q_k)^2]^2}\frac{8\pi V}{(2\pi c)^3}\omega_k^2\,d\omega_k$$
$$\approx\mu_2\left[\frac{4P_c\omega^2}{c^3}\right]^2\frac{1}{\pi N_s}=\frac{\mu_2}{\bar{\epsilon}^2}\left[\frac{8\pi}{V}\frac{Q}{\omega}\bar{\epsilon}N_s\frac{\pi}{2}AS\right]^2\frac{1}{\pi N_s}, \tag{48}$$

where $\bar{\epsilon}$ is the mean value of ϵ_k, μ_2 is the second moment of ϵ_k ($\mu_2=E[\epsilon_k^2]$), $\omega-\Omega$ and $\omega+\Omega$ are the cutoff frequencies for the resonance function, and N_s is the same as defined in Eq. (3). Details of the integration can be found in the Appendix.

The second expectation value in Eq. (47) can also be evaluated using the Riemann integral approximation. The cosine term is dependent on the phase lag for each mode which is in turn dependent on the mode's distance in frequency from resonance. The phase for a given mode is

$$\tan(\phi_k)=\frac{\omega^2}{Q_k[\omega^2-\omega_k^2]}\approx\frac{\omega}{2Q_k(\omega-\omega_k)}. \tag{49}$$

The second expectation value in Eq. (47) is first converted to continuous form, followed by substitution of Eq. (49) to convert the integral from ω to ϕ as follows:

$$E\left[\sum_k \sum_l B_{0k}^2 B_{0l}^2 \cos^2(\phi_k-\phi_l)\right] \approx \left[\frac{2\epsilon P_c}{\pi c^3 Q}\right]^2 \int_{\omega-\Omega}^{\omega+\Omega}\int_{\omega-\Omega}^{\omega+\Omega} \frac{\omega_k^3\omega_l^3\cos^2(\phi_k-\phi_l)d\omega_k d\omega_l}{[(\omega-\omega_k)^2+(\omega_k/2Q_k)^2][(\omega-\omega_l)^2+(\omega_l/2Q_l)^2]}$$

$$\approx \left[\frac{4\epsilon P_c\omega^2}{c^3}\right]^2 \int_{0-\delta}^{-\pi+\delta}\int_{0-\delta}^{-\pi+\delta} \cos^2(\phi_k-\phi_l)d\phi_k d\phi_l = \left[8\pi\frac{U}{V}\right]^2\frac{1}{2}\ . \tag{50}$$

Details of the integration again follow in the Appendix. Equations (48) and (50) can be inserted into Eq. (47) yielding

$$\sigma^2=\alpha\beta^2=\left[\sigma_s\frac{Uc}{3V}\right]^2\left[1+\frac{1}{\pi N_s}\left[\frac{3}{2}\frac{\mu_2}{\bar{\epsilon}^2}+3\frac{\sigma_\epsilon^2}{\bar{\epsilon}^2}\right]\right]$$

$$=\alpha^2\beta^2\left[1+\frac{1}{\pi N_s}\left[\frac{3}{2}\frac{\mu_2}{\bar{\epsilon}^2}+3\frac{\sigma_\epsilon^2}{\bar{\epsilon}^2}\right]\right]. \tag{51}$$

As a result of the fact that the ϵ_k are gap statistics, it can be shown that

$$\frac{\mu_2}{\bar{\epsilon}^2}\approx 2\ ,$$
$$\frac{\sigma_\epsilon^2}{\bar{\epsilon}^2}\approx 1\ , \tag{52}$$

and

$$\sigma^2=\left[\sigma_s\frac{Uc}{3V}\right]^2\left[1+\frac{6}{\pi N_s}\right]. \tag{53}$$

Solving for α and β we find

$$\alpha(\omega)=\left[1+\frac{6}{\pi N_s}\right]^{-1}, \tag{54}$$

$$\beta(\omega)=\mu\left[1+\frac{6}{\pi N_s}\right], \tag{55}$$

$$\mu(\omega)=\alpha\beta=E[P_s(\omega)]=\sigma_s\frac{Uc}{3V}\ , \tag{56}$$

where we have again expressed Eq. (56) in practical cgs units.

From Eq. (56) an expression for the mean Q of a complex cavity can be derived in terms of measurable quantities:

$$Q=\frac{\omega U}{P_c}=\frac{3\omega V}{\sigma_s c}\frac{E(P_s(\omega))}{P_c}\approx\frac{3\omega V}{\sigma_s c}\frac{E(P_s(\omega))}{P_c}\ , \tag{57}$$

where P_c is the input power to the cavity in ergs/sec. If a transfer function is measured to a single point in a cavity it is best to assume $g(\mathbf{r})=1$ since that is its expectation value when measured over many points in the cavity. If the transfer function is measured at several points in the cavity it is still best to use $g(\mathbf{r})=1$, but use the mean value of all of the transfer functions to determine the ratio of the expectation value of the sensor signal to the input power.

If a test object is being illuminated from the outside, P_c is not well defined since it depends on the incident power density and the effective coupling area. However, this problem is easily overcome by a technique developed at JAYCOR called direct cavity pumping. In this technique an antenna is placed inside the cavity, so that all of the power radiated is coupled to the cavity. In this case P_c is all of the power radiated by the antenna and may be easily related to the source power. In reality some power is also absorbed by the antenna. In practice the Q of virtually all cavities of real systems, which are not designed to be high Q resonators, are low enough that the additional losses out of the cavity pumping antenna are negligible. If it is necessary to quantify the magnitude of the losses due to the antenna relative to other losses in the cavity, a circulator can be placed in line behind the antenna and the antenna's absorbed power can be measured. Care must be taken to account for small reflections of the source power due to mismatches between the cable and antenna impedances. These reflected signals are large enough to be confused with the small signal reabsorbed from the cavity. Another point of caution when measuring cavity Q by this technique is that the sensor (B-dot, etc.) should not be placed in direct line with the beam from the antenna. If it is, an incorrect measurement will result. It is best to orient the source antenna at an odd angle relative to any regular walls of the cavity. It is even better to point the antenna at some very irregular object in the cavity which will scatter the radiation and cause it to couple to many modes.

COMPARISON OF THEORY WITH EXPERIMENT

The object of this work is to relate quantities commonly measured in high-power-microwave (HPM) experiments (transfer functions and cross sections) to quantities of practical and theoretical interest (probability of component kill, cavity Q, prediction of cavity field statistics for objects unavailable for test, etc.). For this work to be useful, good agreement must be obtained between this theory and experimental data. First, the theory predicts that in the limit of large cavity volume and/or low Q that the specific mode density of the cavity becomes large and α goes to 1 [Eq. (54)]. The Γ distribution with α equal to 1 is called a χ^2 distribution with two degrees of freedom, or an exponential distribution. In this limit the distribution becomes independent of the cavity's details, including its volume and Q, and becomes what one might call a

"universal distribution." The only parameter which the distribution depends on is its mean value.

The first example that is used to illustrate the comparison of the theory with actual data is a copper cavity $24\times24\times36$ in.^{3}. A field is excited inside the cavity by cw illumination, and is measured by a B-dot sensor inside the cavity. Figure 1 is a plot of the transfer function derived from this data. Figure 2 is a comparison of the empirical cumulative distribution function (CDF) with the theoretical χ^2 distribution with two degrees of freedom.

A number of distribution functions have been used to empirically fit microwave transfer function CDF's. Among the most popular have been CDF's of Gaussian and logarithmic normal distributions. To compare the cumulative distribution functions of a transfer function for a large test object, using different distributional assumptions, probability plots are used. For the measured data, comparisons of fit to χ^2, Gaussian, and logarithmic normal distributions are studied in this way. A probability plot displays the inverse theoretical probability versus the inverse measured probability. A perfect match between theory and experiment produces a diagonal straight line. The dotted curved lines on either side of the diagonal are 90% confidence limits derived using Kolmogorov test statistics for the distribution shown in each plot. If the distribution is correct the entire probability curve should fall within the limits for 90% of all data sets. The spread in the confidence limits at either end is the result of statistical uncertainty in the measured data due to the small number of measured points yielding very small or very large values. Figure 3 is the probability plot for the data in Fig. 1, assuming a χ^2 distribution, Fig. 4 assumes a Gaussian distribution, and Fig. 5 assumes a logarithmic normal distribution.

As seen in Fig. 3, the χ^2 distribution is clearly the best fit to the sample of empirical data. In this case the data fell outside the confidence limits for both the Gaussian and the logarithmic normal distributions on the first data set tested. This indicates with high probability that Gaussian and logarithmic normal distributions are not correct for this type of data.

One of the results of this theory which makes it most useful is the fact that under very general conditions, the

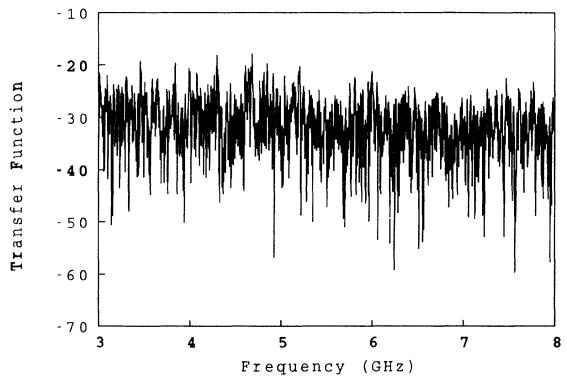

FIG. 1. Transfer function in copper cavity.

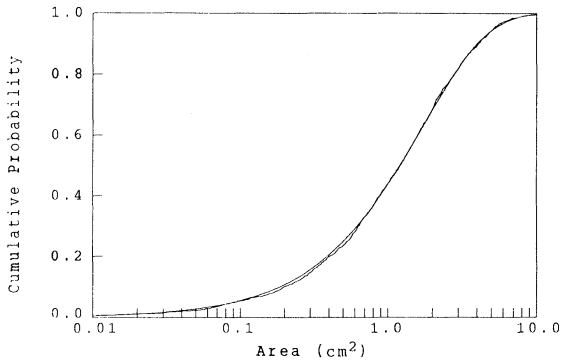

FIG. 2. Empirical and χ^2 CDF's.

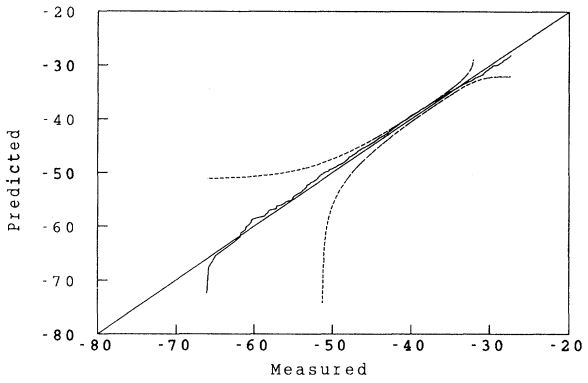

FIG. 3. χ^2 distribution.

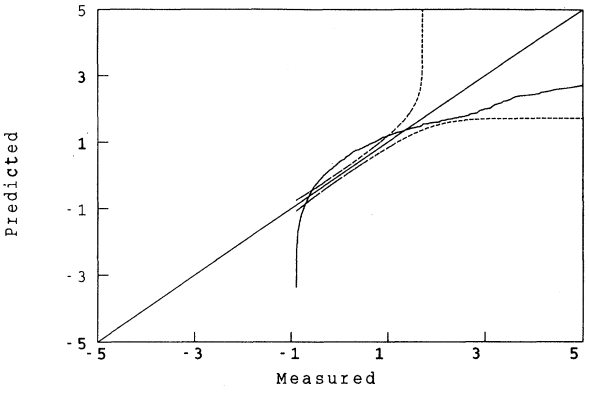

FIG. 4. Gaussian distribution.

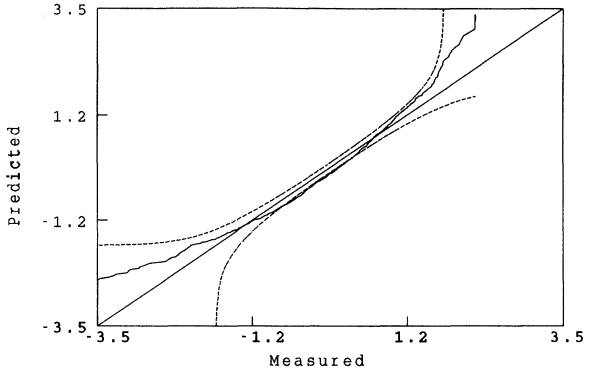

FIG. 5. Logarithmic normal distribution.

CDF does not depend on details of the cavity. Large computer codes have been formulated to model cavities to extremely fine detail. Results of such an approach require extensive amounts of computer time, only to be invalidated if the operator in the test object were to be holding, say, a cola can at the time. To illustrate the fact that the shape of the CDF would not deviate from the theoretical χ^2 distribution, the experiment in Fig. 1 was repeated, but with a cola can half full of water in the cavity. Figure 6 is the probability plot for the χ^2 distribution for the transfer function measured with a cola can present.

The χ^2 distribution with two degrees of freedom appears elsewhere as the probability distribution for amplitude spectra. If a time series is weakly stationary, the periodogram is known to be distributed as χ^2 with two degrees of freedom (Refs. [8,9]). If the system under study is taken as a linear, time invariant filter (the basis for cw analysis), and is excited by a white noise source, then the resulting time domain signal is a weakly stationary time series with spectra identical to the transfer function. The difference is that in the case of the weakly stationary time series, a single fixed filter is driven by a broadband random source, while in the cw amplitude case a single monochromatic source is assumed to be driving randomly selected filters. The two cases can be related if for each possible white noise input into the system, there exists one and only one corresponding cw amplitude measurement such that the discrete Fourier transform of the resulting time domain signal has amplitude spectra identical to the corresponding cw measured amplitude spectra. If this assumption is true, then it follows that the cw amplitude spectra will be distributed as a χ^2 with two degrees of freedom. This assumption has been used successfully to generate a probability model for cw amplitude spectra for electromagnetic-pulse (EMP) excitation of the TACAMO and EMPTAC aircraft (see Ref. [10]). This assumption is being studied further as the basis for an alternative proof of the distribution for amplitude spectra. This proof will also apply to EMP broadband excitation.

To challenge further the validity of the theory described above we have taken data from a wide variety of test objects with various volumes, Q's, sizes, and shapes. Figure 7 shows the transfer function measured in a large

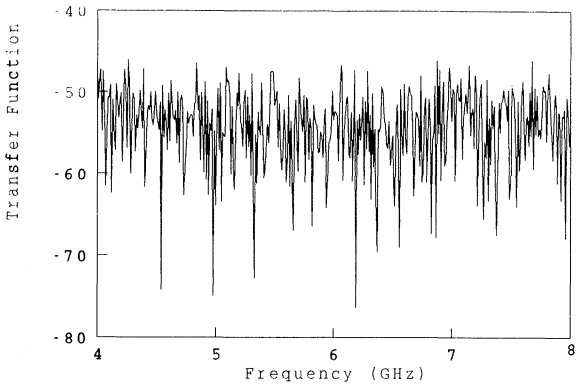

FIG. 7. Large test chamber.

steel box using the direct cavity pumping technique. The volume of the box was 18×10^6 cm^3. A number of irregularly shaped metal objects, including chairs, were placed in the box to prevent any mode degeneracy due to the fairly regular shape of the box. Measurements made with and without cavity clutter showed no significant difference.

In addition, varying amounts of microwave absorber were added to the box to change its Q. Measurements were made with no absorber on the walls, absorber partially covering the walls, and absorber covering virtually the entire surface of the walls. Absolute measurements of source and sensor power were made and the Q was derived using Eq. (57). Figure 8 shows the probability plot for the χ^2 distribution, using measurements with no absorber other than normal wall losses. The cavity Q was 5400 and the specific mode density was about 670. As shown the fit between theory and experiment was excellent. Figure 9 shows the probability plot using data for the lightly damped steel chamber. The measured Q was 378 and the specific mode density was about 9600. The fit between theory and data was again very good. Figure 10 shows the probability plot for the data for the heavily damped steel chamber. The measured Q was 88 and the specific mode density was 41 000. The fit to data was still excellent. The range of cavity Q's tested with the steel chamber covers virtually the entire range found in real systems. The data shown in Fig. 7 are also tested using

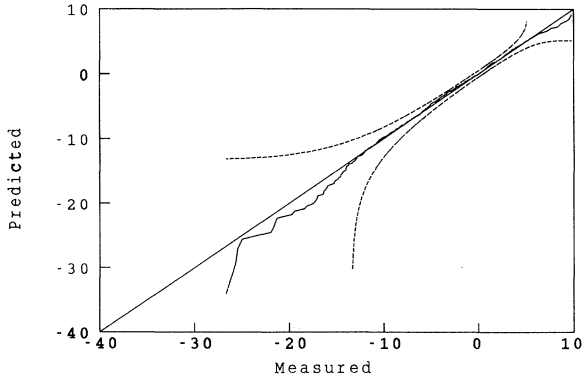

FIG. 6. Copper cavity with cola can.

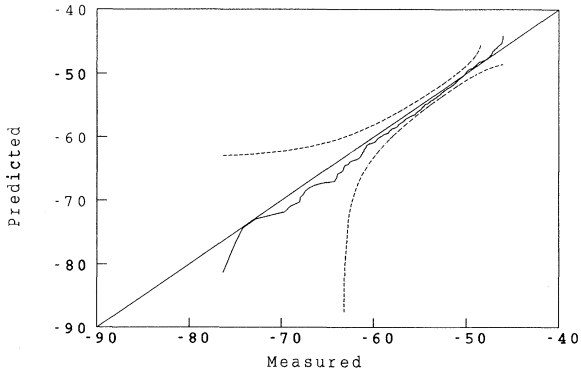

FIG. 8. Chamber without echosorb.

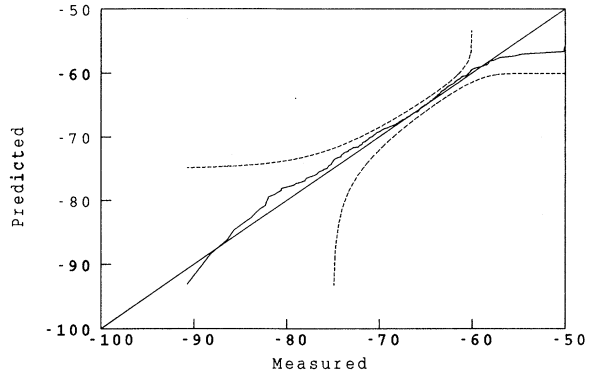

FIG. 9. Partial echosorb.

Gaussian and logarithmic normal distributions. Figure 11 is the probability plot for a Gaussian distribution, and Fig. 12 is the probability plot for a logarithmic normal distribution. As can be seen, both distributional assumptions are violated.

To challenge the theory with real test articles rather than contrived laboratory cavities, we made measurements on a small computer, an air to ground missile, a fighter jet aircraft, a Cessna Citation Jet, a large transport aircraft, and a large military ground vehicle. The volumes of the various cavities varied by over a factor of 1000. The probability plots for the χ^2 distribution for the first five test objects, illustrating the excellent agreement between theory and data, are shown in Fig. 13–17. Agreement between theory and experimental data over such a broad range of size, shape, and Q lends considerable support to the validity of the theory. However, all of the objects tested above challenged the theory in the limit of large specific mode density. We have, to date, measured a few objects in the limit of low specific mode density and shown that α does indeed differ from 1, however, we have not yet completed quantitative verification of the theory in the low-specific-mode-density limit.

DETECTION AND CORRECTION OF DISTORTED DATA

The data described by this theory cover many orders of magnitude and sometimes exceed the limits of dynamic

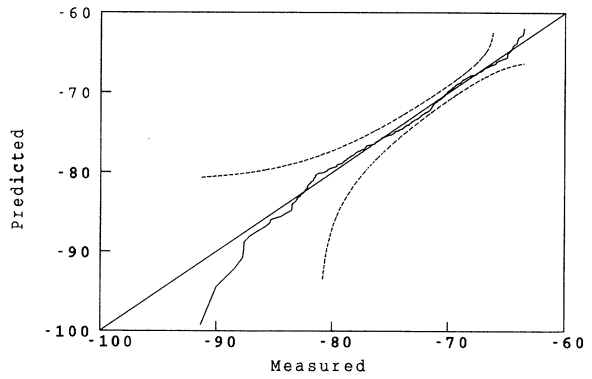

FIG. 10. Fully damped with echosorb.

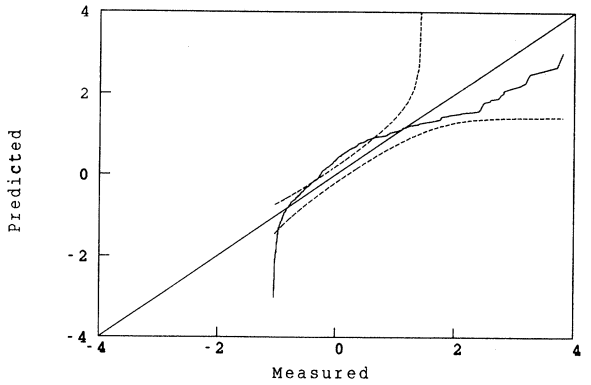

FIG. 11. Large test chamber, Gaussian.

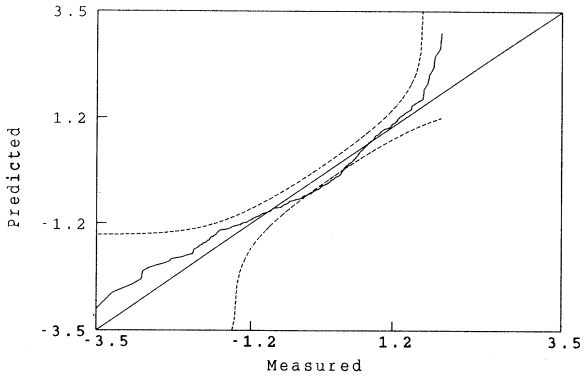

FIG. 12. Large test chamber, logarithmic normal.

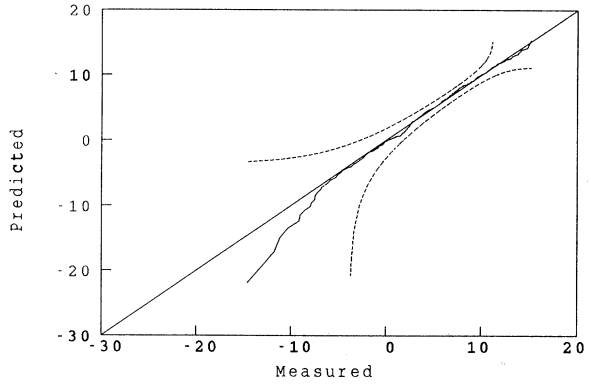

FIG. 13. Power supply in computer.

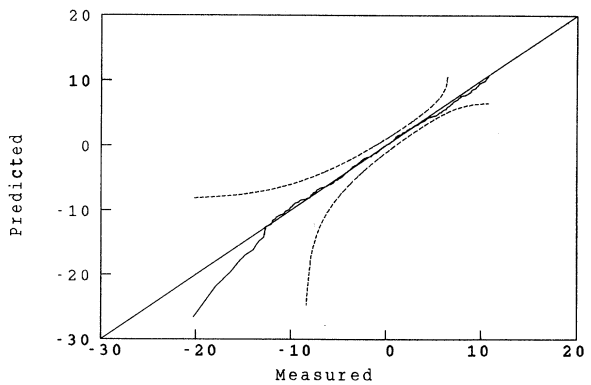

FIG. 14. Air-to-ground missile.

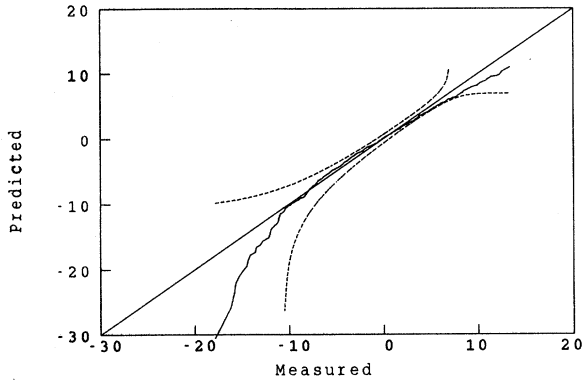

FIG. 15. Fighter-jet aircraft fuselage.

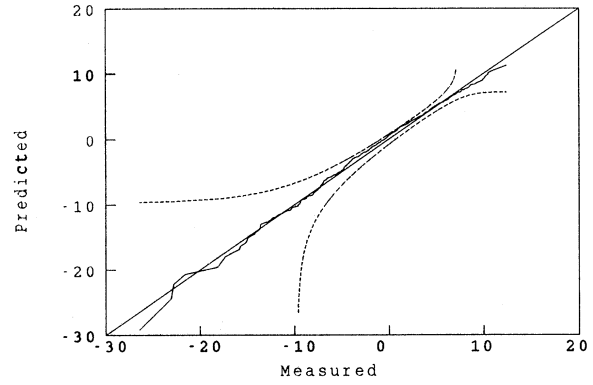

FIG. 16. Cessna Citation aircraft fuselage.

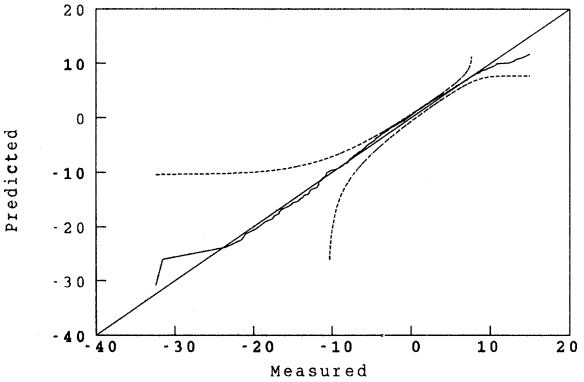

FIG. 17. Large-transport-aircraft cockpit.

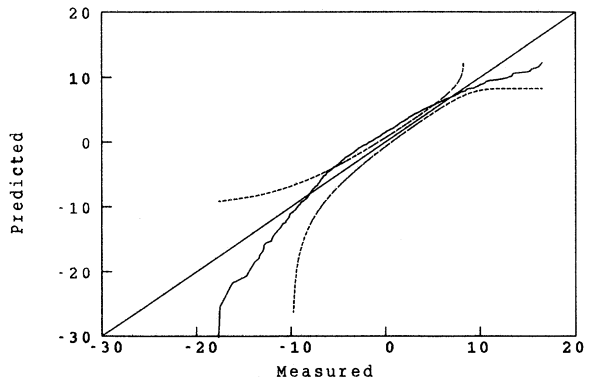

FIG. 18. Large ground vehicle, mean extracted.

range of the instruments used to acquire the data. Some of the lowest-amplitude signals can be below the noise level of the instrument. This distorts the low-end tail and shifts the mean of the distribution, which is used to estimate the location parameter of the exponential distribution. We have observed this effect in some of our data where the signals were particularly low. The effect of this distortion on the probability plot is shown in Fig. 18 for data taken from the gunner's chamber of a large military ground vehicle. If it is known that the cavity under test is in the large-specific-mode-density limit ($N_s > 10$) the distortion can be easily detected and corrected.

While the mean of the distribution is affected by the limited dynamic range of the measurement, the median is unchanged. This is because the mean weights each point by its deviation from the center, but the median is simply the value at which half the measured points are above and half below. Clipping the low points changes the weighting that determines the mean, but does not change the number of points below the median value. In fact, the signal can be clipped up to the median value without the median being changed. In the limit of large N_s the shape of the distribution is determined by only one parameter, the mean. For the Γ distribution with $\alpha=1$, the mean and the median are related by a constant ratio:

$$\beta=\mu=E[P_s]=\frac{P_{s,[0.50]}}{\ln(2)}\ , \tag{58}$$

where the $P_{s,[0.50]}$ indicates median value. When the data are distorted by limited dynamic range, the median, which is unchanged, can be used to recover the correct mean value using Eq. (58) and restore the low-end tail of the distribution function. The probability plot from Fig. 18 is shown corrected by this technique in Fig. 19. Note that the error of only 3 dB in Fig. 18 was easily detected and corrected. It is also possible to use this relation to generate an alarm during automatic data acquisition to notify the operator when a specified level of distortion is exceeded. Equation (58) is not the optimum statistical estimator for distortion of the low-end tail. We are currently developing other more sensitive and accurate estimators to detect measurement errors and detect deviations of experimental data from theoretical expectations.

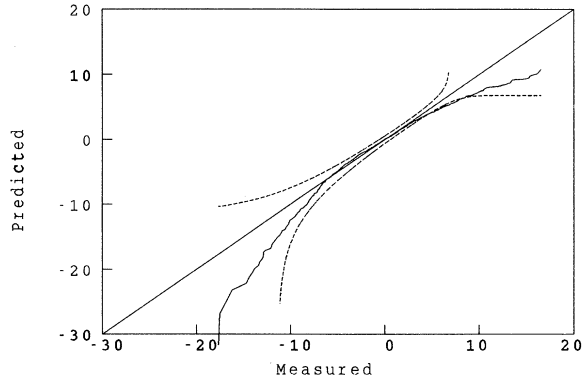

FIG. 19. Large ground vehicle, median extracted.

ACKNOWLEDGMENTS

R.H.P. thanks Marilyn Glaubensklee for stimulating questions and discussions during the early development of this work. The authors are also indebted to Ted Lehmann for finding an error in the original formulation of Eq. (36).

APPENDIX: DETAILS OF INTEGRATION

Equations (37), (48), and (50) involve solving complicated integrals, and to simplify the paper, the details of these integrations are explained here. Two approaches will be used, the first a quick approximation by considering the Laurent's function to be approximated by a δ function. Then the value of the rest of the function, evaluated at the center of the Laurent's function, will be brought out of the integral. The second method is much more laborious, and gives an exact solution which will be truncated to give the same value as the quick approximation.

Equation (37): Solve

$$\frac{2\pi\bar{\epsilon}P_c}{QV}\frac{8\pi V}{(2\pi c)^3}\int_{\omega-\Omega}^{\omega+\Omega}\frac{\omega_k^3}{(\omega_k-\omega)^2+(\omega/2Q)^2}d\omega_k \ . \tag{A1}$$

Considering the Laurent's function in the denominator to be a δ function centered about ω, we get the approximation

$$\int_{-\infty}^{\infty}\frac{\omega_k^3}{(\omega_k-\omega)^2+(\omega/2Q)^2}d\omega_k \approx \omega^3\int_{-\infty}^{\infty}\frac{d\omega_k}{(\omega_k-\omega)^2+(\omega/2Q)^2} \ . \tag{A2}$$

To solve the latter integral, first make the change of variable $u=\omega_k-\omega$:

$$\int_{-\infty}^{\infty}\frac{d\omega_k}{(\omega_k-\omega)^2+(\omega/2Q)^2}=\int_{-\infty}^{\infty}\frac{du}{u^2+a} \ , \tag{A3}$$

where $a=(\omega/2Q)^2$. Using Sec. 2.172 of Ref. [11],

$$\int_{-\infty}^{\infty}\frac{du}{u^2+a}=\frac{2\pi Q}{\omega} \tag{A4}$$

and

$$\int_{-\infty}^{\infty}\frac{\omega_k^3}{(\omega_k-\omega)^2+(\omega/2Q)^2}d\omega_k\approx 2\pi Q\omega^2 \ , \tag{A5}$$

which combines with Eqs. (A1) and (A2) to get

$$\frac{2\pi\bar{\epsilon}P_c}{QV}\frac{8\pi V}{(2\pi c)^3}\int_{\omega-\Omega}^{\omega+\Omega}\frac{\omega_k^3}{(\omega_k-\omega)^2+(\omega/2Q)^2}d\omega_k\approx\frac{4\bar{\epsilon}P_c\omega^2}{c^3} \ . \tag{A6}$$

To solve the integral exactly, first make the change of variable as before, $u=\omega_k-\omega$:

$$\begin{aligned}\int_{\omega-\Omega}^{\omega+\Omega}\frac{\omega_k^3}{(\omega_k-\omega)^2+(\omega/2Q)^2}d\omega_k &= \int_{-\Omega}^{\Omega}\frac{(u+\omega)^3}{u^2+a}du \\ &= \int_{-\Omega}^{\Omega}\frac{u^3+3u^2\omega+3u\omega^2+\omega^3}{u^2+a}du \ .\end{aligned} \tag{A7}$$

Since the denominator is symmetric, the odd powers will integrate to zero

$$\int\frac{u}{u^2+a}du=\int\frac{u^3}{u^2+a}du=0 \ . \tag{A8}$$

Using Sec. 2.175 of Ref. [11], it follows that

$$\int_{-\Omega}^{\Omega}\frac{u^2}{u^2+a}du=2\Omega-\frac{\omega\pi}{2Q} \ . \tag{A9}$$

Using Eqs. (A4) and (A8), Eq. (A6) can be solved:

$$\begin{aligned}\int_{\omega-\Omega}^{\omega+\Omega}\frac{\omega_k^3}{(\omega_k-\omega)^2+(\omega/2Q)^2}d\omega_k &= \int_{-\Omega}^{\Omega}\frac{u^3+3u^2\omega+3u\omega^2+\omega^3}{u^2+a}du \\ &= 3\omega\left[2\Omega-\frac{\omega\pi}{2Q}\right]+\omega^3\frac{2\pi Q}{\omega} \\ &= 2\pi Q\omega^2+3\omega\left[2\Omega-\frac{\omega\pi}{2Q}\right] \ .\end{aligned} \tag{A10}$$

and it can be seen that the lead term of Eq. (A10) agrees with Eq. (A5). Putting it all together,

$$\frac{2\pi\bar{\epsilon}P_c}{QV}\frac{8\pi V}{(2\pi c)^3}\int_{\omega-\Omega}^{\omega+\Omega}\frac{\omega_k^3}{(\omega_k-\omega)^2+(\omega/2Q)^2}d\omega_k = \frac{4\bar{\epsilon}P_c\omega^2}{c^3}\left[1+\frac{3\Omega}{\pi\omega Q}-\frac{3}{4Q^2}\right] \tag{A11}$$

and since $\Omega<\omega$, and $Q>1$, the lead term in Eq. (A11) clearly dominates. Actual calculations have found the error of approximation to be less than 2%.

Equation (49): Solve

$$\int_{\omega-\Omega}^{\omega+\Omega}\frac{\left[\frac{2\pi\bar{\epsilon}P_c\omega_k}{QV}\right]^2}{[(\omega_k-\omega)^2+(\omega/2Q)^2]^2}\frac{8\pi V}{(2\pi c)^3}\omega_k^2 d\omega_k \ . \tag{A12}$$

Using again the approximation of the denominator being a δ function, the same change of variable, and Sec. 2.173 of Ref. [11],

$$\begin{aligned}\int_{-\infty}^{\infty}\frac{\omega_k^4}{[(\omega_k-\omega)^2+(\omega/2Q)^2]^2}d\omega_k &\approx \omega^4\int_{-\infty}^{\infty}\frac{du}{[u^2+a]^2} \\ &= \omega^4\left[\frac{4\pi Q^3}{\omega^3}\right] \\ &= 4\pi Q^3\omega \ .\end{aligned} \tag{A13}$$

To solve the equation explicitly, make the usual change of variable:

$$\int_{\omega-\Omega}^{\omega+\Omega}\frac{\omega_k^4}{[(\omega_k-\omega)^2+(\omega/2Q)^2]^2}$$
$$=\int_{-\Omega}^{\Omega}\frac{(u+\omega)^4}{[u^2+a]^2}du$$
$$=\int_{-\Omega}^{\Omega}\frac{u^4+4u^3\omega+6u^2\omega^2+4u\omega^3+\omega^4}{[u^2+a]^2}du\ , \tag{A14}$$

and again, since the denominator is symmetric, the odd powers integrate to zero. Using Ref. [11], it can be shown that

$$\int\frac{du}{[u^2+a]^2}du=\frac{4\pi Q^3}{\omega^3}+\frac{4Q^2}{\omega^2}\frac{\Omega}{\Omega^2+a}$$
$$\approx\frac{4\pi Q^3}{\omega^3}\ , \tag{A15}$$

$$\int\frac{u^2}{[u^2+a]^2}du=\frac{\pi Q}{\omega}-\frac{\Omega}{\Omega^2+a}$$
$$\approx\frac{\pi Q}{\omega}\ , \tag{A16}$$

where both equations used the fact that $\Omega\gg1$. It can also be shown that

$$\int\frac{u^4}{[u^2+a]^2}du=\frac{3\pi\omega}{4Q}+2\Omega\ . \tag{A17}$$

Using Eqs. (A15)–(A17) to solve Eq. (A14),

$$\int_{-\Omega}^{\Omega}\frac{u^4+4u^3\omega+6u^2\omega^2+4u\omega^3+\omega^4}{[u^2+a]^2}du$$
$$=\frac{3\pi\omega}{4Q}+2\Omega+6\pi Q\omega+4\pi Q^3\omega$$
$$=4\pi Q^3\omega\left[1+\frac{3}{2Q^2}+\frac{3}{16Q^4}+\frac{\Omega}{2\pi\omega Q^3}\right]\ , \tag{A18}$$

and again, the facts that $\Omega<\omega$, and $Q>1$ makes the lead term in Eq. (A18) dominate. This agrees with the approximation in Eq. (A13).

Equation (51): Solve

$$\int_{\omega-\Omega}^{\omega+\Omega}\int_{\omega-\Omega}^{\omega+\Omega}\frac{\omega_k^3\omega_l^3\cos^2(\phi_k-\phi_1)}{[(\omega_k-\omega)^2+(\omega/2Q)^2][(\omega_l-\omega)^2+(\omega/2Q)^2]}d\omega_k d\omega_l\ . \tag{A19}$$

This integral is simplified by using the transformation

$$\tan(\phi_k)=\frac{\omega}{2Q(\omega-\omega_k)}\ , \tag{A20}$$

then

$$d\omega_k=\frac{\omega}{2Q\sin^2(\phi_k)}d\phi_k \tag{A21}$$

and

$$\frac{1}{(\omega-\omega_k)^2+(\omega/2Q)^2}=\left[\frac{2Q}{\omega}\right]^2\sin^2(\phi_k)\ . \tag{A22}$$

First approximating the integral using the denominator as a δ function,

$$\int_{-\infty}^{\infty}\int_{-\infty}^{\infty}\frac{\omega_k^3\omega_l^3\cos^2(\phi_k-\phi_l)}{[(\omega-\omega_k)^2+(\omega/2Q)^2][(\omega-\omega_l)^2+(\omega/2Q)^2]}d\omega_k d\omega_l\approx4Q^2\omega^4\int_0^{\pi}\int_0^{\pi}\cos^2(\phi_k-\phi_l)d\phi_k d\phi_l$$
$$=\pi^2Q^2\omega^4\ . \tag{A23}$$

The exact integral uses the same transformation, however, the ω_k^3 factors out as a result of the fact that

$$\omega_k^2=\omega^2\left[1-\frac{1}{Q\tan(\phi_k)}\right] \tag{A24}$$

and so

$$\mathcal{J}\equiv\int_{\omega-\Omega}^{\omega+\Omega}\int_{\omega-\Omega}^{\omega+\Omega}\frac{\omega_k^3\omega_l^3\cos^2(\phi_k-\phi_l)}{[(\omega-\omega_k)^2+(\omega/2Q)^2][(\omega-\omega_l)^2+(\omega/2Q)^2]}d\omega_k d\omega_l$$

$$=\left[\frac{2Q}{\omega}\right]^2\omega^6\int_\delta^{\pi-\delta}\int_\delta^{\pi-\delta}\left[1-\frac{1}{Q\tan(\phi_k)}\right]^{3/2}\left[1-\frac{1}{Q\tan(\phi_l)}\right]^{3/2}\cos^2(\phi_k-\phi_l)d\phi_k d\phi_l$$

$$=4Q^2\omega^4\int_\delta^{\pi-\delta}\int_\delta^{\pi-\delta}\left[1-\frac{1}{Q\tan(\phi_k)}\right]^{3/2}\left[1-\frac{1}{Q\tan(\phi_l)}\right]^{3/2}[\cos(\phi_k)\cos(\phi_l)+\sin(\phi_k)\sin(\phi_l)]^2d\phi_k d\phi_l \tag{A25}$$

and expanding the square,

$$\mathcal{J}=(2Q)^2\omega^4\left[\int_\delta^{\pi-\delta}\left[1-\frac{1}{Q\tan(\phi)}\right]^{3/2}\cos^2(\phi)d\phi\right]^2+(2Q)^2\omega^4\left[\int_\delta^{\pi-\delta}\left[1-\frac{1}{Q\tan(\phi)}\right]^{3/2}\cos(\phi)\sin(\phi)d\phi\right]^2$$

$$+(2Q)^2\omega^4\left[\int_\delta^{\pi-\delta}\left[1-\frac{1}{Q\tan(\phi)}\right]^{3/2}\sin^2(\phi)d\phi\right]^2$$

$$=(2Q)^2\omega^4\left[\int_\delta^{\pi-\delta}[\cos^2(\phi)+\cos(\phi)\sin(\phi)+\sin^2(\phi)]d\phi\right]^2+O\left[\frac{1}{Q}\right]$$

$$=\pi^2Q^2\omega^4+O\left[\frac{1}{Q}\right], \tag{A26}$$

which agrees with Eq. (A23).

[1] Russell H. Bonn, Eric P. Wenaas, Robert H. Price, Herbert T. Davis, and Robert Achenbach (unpublished).

[2] E. P. Wenaas and H. T. Davis (unpublished).

[3] R. Eisberg, *Fundamentals of Modern Physics* (Wiley, New York, 1961), pp. 51–57.

[4] Ron Pyke, J. R. Stat. Soc. Ser. B **27**, 395 (1965).

[5] Robert E. Collin, *Foundations for Microwave Engineering* (McGraw-Hill, New York, 1966), p. 328.

[6] Herbert Solomon, in *Proceedings of the Fourth Berkeley Symposium on Mathematical Statistics and Probability, Vol. 1* (University of California Press, Berkeley, CA, 1961), pp. 645–653.

[7] N. G. Gamkrelidge and V. I. Rotar', Theory Probab. Its Appl. (USSR) **22**, 394 (1977).

[8] R. A. Fisher, Proc. R. Soc. London Ser. A **125**, 54 (1929).

[9] E. J. Hannan, *Time Series Analysis* (Methuen, London, 1960), pp. 52–55.

[10] H. T. Davis, N. Engheta, S. A. Kokorowski, J. P. Martinez, D. McLemore, B. J. Moser, L. M. Rose, W. J. Stark, R. E. Thomas, and F. Y. Wong, *EMP Stress Data Analysis, Vol. II: Description of Analysis Procedures* (Kaman Sciences Corp., 1988), pp. 163–189.

[11] I. S. Gradshteyn and I. W. Ryzhik, *Tables of Integrals and Products* (Academic, New York, 1965).